

Multiple light scattering on the $F = 1 \rightarrow F' = 0$ transition in a cold and high density ^{87}Rb vapor

S. Balik, A.L. Win and M.D. Havey

*Department of Physics, Old Dominion University, Norfolk, VA 23529**

A.S. Sheremet, I.M. Sokolov and D.V. Kupriyanov

Department of Theoretical Physics, State Polytechnic University, 195251, St.-Petersburg, Russia

(Dated: November 2, 2021)

We report an experimental study of near resonance light scattering on the $F = 1 \rightarrow F' = 0$ component of the D_2 line in atomic ^{87}Rb . Experiments are performed on spatially bi-Gaussian ultracold gas samples having peak densities ranging from about $5 \cdot 10^{12} - 5 \cdot 10^{13}$ atoms/cm³ and for a range of resonance saturation parameters and detunings from atomic resonance. Time resolution of the scattered light intensity reveals dynamics of multiple light scattering, optical pumping, and saturation effects. The experimental results in steady-state are compared qualitatively with theoretical models of the light scattering process. The steady-state line shape of the excitation spectrum is in good qualitative agreement with these models.

PACS numbers: 42.25.Dd, 42.50.Nn, 42.50.-P, 72.15.Rn, 37.10.Gh

I. INTRODUCTION

The interaction of light with dense atomic gases is a vigorous area of research in quantum optics [1–24]. Part of this interest stems from the interdisciplinary nature of the field, and with the large number of fundamentally important results and potential applications that have emerged. Recent efforts have ranged from basic studies of light localization in disordered systems [25–33], including atomic gases, to investigation of cooperative scattering [34–41]. Areas of experimental and theoretical research with both fundamental motivations and possible applications include searches for atomic physics based random lasing [42–47] and quantum memories for quantum information and communications [48–50]. Single photon optical memories in dense atomic gases may potentially be derived from a number of approaches, including development of subradiant atomic-photonic modes [51], and extensions of electromagnetically-induced-transparency (EIT) based approaches to novel two-photon optical schemes at higher densities [7, 9, 10, 19, 20, 52, 53].

We have ongoing experimental and theoretical research efforts focused in part on developing quantum memories using either two-photon EIT based approaches on one hand [52–56], and on the possible formation of subradiant single photon modes on the other [27–29]. To obtain formation of subradiant modes is a challenging experimental enterprise, and requires atomic densities $\sim 10^{14}$ atoms/cm³, in order to achieve high orders of multiple light scattering in the sample. In addition, dynamical processes which either dephase the multiply scattered light or which lead to reduction in the scattering cross-section should be well understood. The current program is focused on nearly optically closed hyperfine transi-

tions associated with the D_2 transition in ultracold ^{87}Rb . These two transitions are the $F = 2 \rightarrow F' = 3$ main optical trapping component and the $F = 1 \rightarrow F' = 0$ transition arising from the lower energy ground state hyperfine component. We have reported elsewhere our experimental research associated with light scattering on the $F = 2 \rightarrow F' = 3$ transition [57].

In the present paper we report experimental and theoretical investigation of the $F = 1 \rightarrow F' = 0$ transition in ^{87}Rb . Overall, our studies include examination of the roles of atomic density, optical saturation, and detuning of probe radiation from optical resonance on the $F = 1 \rightarrow F' = 0$ transition. We will see that, for this transition, the debilitating effects of Zeeman optical pumping play an essential role in all aspects of the experiments. In the present paper, we concentrate primarily on steady state optical excitation and how the light scattering signals depend in that case on probe detuning and atomic density. In the following sections we first provide some details of our experimental approach. This is followed by presentation of our experimental results and comparative discussion on the basis of theoretical models of the light scattering process.

II. EXPERIMENTAL CONFIGURATION

A schematic diagram of the experimental apparatus used in the measurements is shown in Fig. 1, while the particular optical transitions of interest associated with the atomic ^{87}Rb D_2 line are shown in Fig. 2. As illustrated in Fig. 1, the central part of the experimental apparatus is a magneto optical trap (MOT) which serves to form and confine cold ^{87}Rb atom samples. The MOT is a standard vapor-loaded trap formed in a vacuum chamber with a base pressure $\sim 10^{-9}$ Torr. The six MOT beams are derived from a single external cavity diode laser (ECDL) with the grating arranged in a

*Electronic address: mhavey@odu.edu

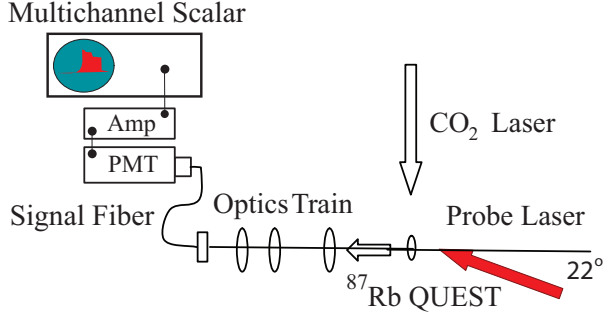


FIG. 1: Schematic diagram of the experimental apparatus. In the figure, PMT refers to an infrared sensitive photomultiplier tube and Amp refers to a fast preamplifier. MOT stands for magneto optical trap, while QUEST is an abbreviation for quasi electrostatic trap.

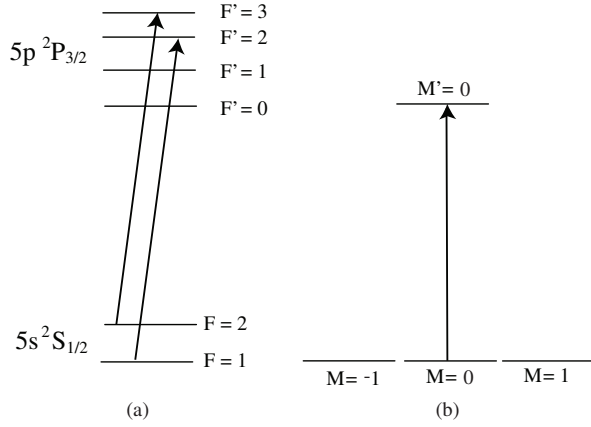


FIG. 2: Energy level diagrams illustrating the experimental scheme. (a) The MOT and repumping transitions used in the present experiment. (b) Probe excitation with linearly polarized light (z-direction) used in the present experiment. In part (b) of the figure, the Zeeman levels have been broken out to show the role of Zeeman optical pumping out of the $F = 1, M = 0$ state to the $F = 1, M = \pm 1$ states.

Littrow configuration. The main master diode laser is frequency locked to a saturation absorption feature produced in a room temperature Rb vapor cell. The master laser power is increased by injecting the master output into slave laser. The arrangement provides more than 20 mW of trapping light in laser beams of cross sectional area $\sim 2 \text{ cm}^2$. The slave laser output is switched and spectrally shifted as required with an acousto optical modulator (AOM) to a frequency set at about 18 MHz below the ^{87}Rb $F = 2 \rightarrow F' = 3$ trapping transition. The repumper laser is also an ECDL of the same basic design as the main MOT laser, and is locked to the $F = 1 \rightarrow F' = 2$ hyperfine transition. The repumper delivers a beam of maximum intensity $\sim 0.6 \text{ mW/cm}^2$ and is delivered along the same optical path as the main trapping laser beams. Switching of the repumper laser is

also controlled with an AOM.

In the experiments reported here, the cold atom sample is initially produced in the higher energy $F = 2$ level. Direct absorption imaging measurements of the peak optical depth on the $F = 2 \rightarrow F' = 3$ transition yielded, for this sample, $b_o \sim 10$ in a Gaussian radius of $r_o \sim 0.45 \text{ mm}$. However, the main sample production goal is to transfer a significant number of the trapped atoms to a carbon-dioxide laser (CO_2) based far off resonance optical dipole trap. The 100 W CO_2 laser based trap operates at a wavelength of $10.6 \mu\text{m}$ and is deeply in the quasistatic trapping regime. This laser is focussed to a radial spot size of $\sim 55 \mu\text{m}$, and a corresponding Rayleigh range of $z_R \sim 750 \mu\text{m}$. The CO_2 laser focal zone is overlapped with the MOT trapping region, while application of the laser beam itself is controlled by a 40 MHz AOM. The atom sample formed in the MOT is compressed and loaded into the quasistatic dipole trap (QUEST) by detuning the MOT master laser 60 MHz to the low frequency side of the trapping transition, while simultaneously lowering the repumper intensity over an order of magnitude. The resulting temporal dark spot MOT loads the atoms predominantly into the lower energy $F = 1$ hyperfine component. The result of this procedure is transfer of about 15 % of the MOT atoms to the QUEST. It is important to note that this transfer efficiency is determined after a QUEST holding period of about 1 second, during which the atomic sample naturally evolves towards thermal equilibrium (this happens through elastic collisions between the confined Rb atoms). Auxiliary measurements of the QUEST principal characteristics after the 1 s hold period, by absorption imaging, parametric resonance [58], and the measured number of atoms transferred show a sample with peak density about $5 \cdot 10^{13} \text{ atoms/cm}^3$ and a temperature of $\sim 65 \mu\text{K}$. The $1/e$ lifetime of the confined atoms is longer than 5 s, and is limited by background gas collisions. The residual magnetic field in the sample area, when the MOT quadrupole field is switched off, is estimated to be less than a few mG.

In the main experimental protocol, a probe beam tuned in the spectral vicinity of the $F = 1 \rightarrow F' = 0$ nearly closed transition is directed towards the sample, and the resulting scattered light signals collected as illustrated schematically in Fig. 1. The probe laser is of the same design as the repumper laser, has a bandwidth $\sim 3 \text{ MHz}$, and is switched and directed by an acousto optical modulator towards the sample. Because of constraints on the vacuum chamber geometry, the linearly polarized probe beam is directed (see Fig. 1) at an angle of approximately 30 degrees away from the fluorescence collection direction. The probe beam is also directed downwards towards the sample at an angle of 22.5 degrees (as shown in Fig. 1). Finally, the sample fluorescence is collected without regard to light polarization; as light scattering is dominated by the $F = 1 \rightarrow F' = 0$ transition we expect the scattered light to be mainly unpolarized (very small contributions from the quite far off resonance $F = 1 \rightarrow F' = 1, 2$ transitions are in general

| Peak b_t | n_o (atoms/cm ³) | r_o (μ m) | z_o (μ m) |
|------------|--------------------------------|------------------|------------------|
| 40 | 5.0×10^{13} | 9.8 | 248 |
| 28 | 2.5×10^{13} | 13.8 | 248 |
| 20 | 1.2×10^{13} | 19.5 | 248 |
| 13 | 5.1×10^{12} | 30.4 | 249 |

TABLE I: QUEST parameters relating the peak transverse optical depth on the $F = 1 \rightarrow F' = 0$ transition to the maximum sample density and the Gaussian radii of the atomic cloud.

polarized in the single scattering limit).

To close this section, we point out that in some of the experiments reported here the atomic density was varied over a factor of about 10. This was accomplished by allowing for a period of ballistic expansion of the cloud after the QUEST was turned off. The atomic sample temperature is known (by ballistic expansion measurements), so this procedure allows the peak density or the peak optical depth to be determined. As the sample is well approximated by a two-axis Gaussian atom distribution [59], the two Gaussian radii and the peak atom density (or the total number of atoms in the sample), are sufficient to determine the two peak optical depths characterizing the sample. We summarize in Table 1 the peak transverse optical depth b_t the peak atom density at the center of the sample n_o , the transverse Gaussian radius r_o , and the longitudinal Gaussian radius z_o . The optical depth refers here to that of the nearly closed $F = 1 \rightarrow F' = 0$ hyperfine transition, which has a total resonance light scattering cross section of $3.23 \times 10^{-10} \text{ cm}^2$.

III. RESULTS AND DISCUSSION

In this section we present results associated with on-resonance light scattering, where on-resonance refers to the bare-atom $F = 1 \rightarrow F' = 0$ hyperfine resonance frequency, and with variations around that frequency. We emphasize that the measurements are made at a fixed single angle with respect to the incident probe laser; the geometrical setup is described in the previous section. With this in mind, we first expect that the scattered light will be unpolarized, as the excited level has $F' = 0$. However, because of the high optical depth of the sample, the scattered light intensity should show important angular dependence [29, 54, 60]. For instance, light scattered in the near forward direction shows a minimum in the spectral variations near the resonance line center. This can effect the time evolution of the scattered light signals as well [54]. On the other hand, light scattered in the backwards direction shows an enhancement due to the coherent backscattering effect. This spatially cone shaped feature depends critically on probe laser intensities near saturation and also on the spectral detuning from atomic resonance.

A. On-resonance scattering

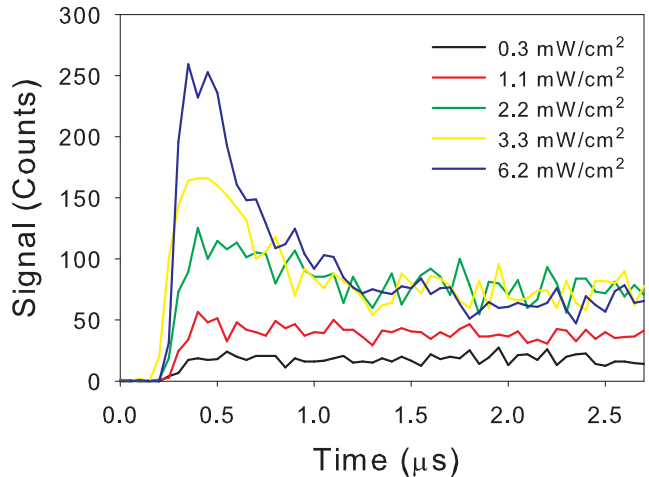


FIG. 3: Time evolution of the probe scattered light intensity on the $F = 1 \rightarrow F' = 0$ hyperfine transition. The atomic density is at its peak level for these measurements. Signals are shown for several different probe laser intensities. The role of optical pumping is apparent at the larger probe intensities. Probe detuning from resonance $\Delta = 0$.

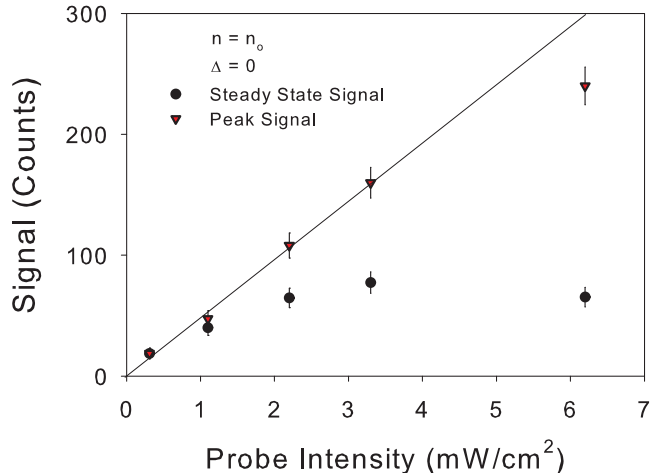


FIG. 4: Variation of the peak and steady state signal levels as a function of the probe laser intensity. Atomic density is at its maximum value n_o for these data. Probe detuning from resonance $\Delta = 0$.

We start by presenting in Fig. 3 the results of typical measurements of the time dependence of light scattered from the atomic sample. These measurements are made for a maximum density sample, which in this case has a transverse optical depth of $b_t \sim 40$, and a peak atom density at the center of the sample of $5.0 \cdot 10^{13} \text{ atoms/cm}^3$. These measurements are made for a range of probe laser

intensities, which for the most part are well below the saturation intensity $I_{sat} \sim 14 \text{ mW/cm}^2$ for linearly polarized excitation of the $F = 1 \rightarrow F' = 0$ transition. We see for higher probe laser intensities a quite rapid buildup to a peak intensity followed by a decay of about $1 \mu\text{s}$ to a steady state. The build up time is less than about 100 ns , and is limited by the turn-on time of the switching AOM used to control application of the probe laser to the sample. We also note that as the probe laser intensity is reduced, the transient peak is reduced, and for the lowest probe laser intensities the scattering signal smoothly rises to a steady value. The overall behavior is summarized in Fig. 4, where the nearly linear growth of the peak in the scattering signal, and the leveling off of the steady state signal is shown. This general behavior of the transient response and the variations of the response with probe laser intensity was found to be qualitatively the same for a range of densities from $0.1n_o$ up to the peak density n_o (see Table 1).

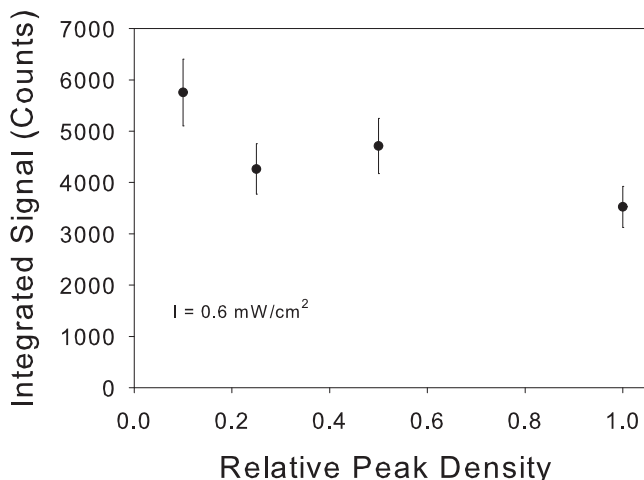


FIG. 5: Variation of the total scattered signal intensity due to systematic changes in the atomic density. Probe detuning from resonance $\Delta = 0$.

As the maximum laser intensity used in these experiments is well below the optical saturation intensity, we can understand the transient behavior to result from Zeeman optical pumping in the ground level due to elastic Raman transitions to the $F = 1, M = \pm 1$ states. This optical pumping does not completely deplete the $F = 1, M = 0$ state because multiple elastic light scattering allows for a build up of radiation within the atomic sample. This gives rise to optical pumping by the diffuse light in the sample, which competes with direct Zeeman optical pumping by the probe beam and results in a nonzero steady state level for the scattered light signal as seen in Fig. 3 and Fig. 4. This process as considered for a wide range of densities and laser intensities will be treated in a later report. In the present paper we are concerned with the steady state signals for the case where the probe intensity is so weak, and the number of scattered photons so few, that there is no mesoscopic

rearrangement of populations in the $F = 1$ level during realization of a single sample. The main results of this paper, as presented in this and the following section, are recorded under those conditions.

We present in Fig. 5 measurements of the variation of the total scattered light intensity from the $F = 1 \rightarrow F' = 0$ hyperfine transition as a function of systematic changes in the atomic density. These measurements were made at very low probe laser intensity, under conditions selected so that there was no perceptible optical pumping, as in the lowest intensity results shown in Fig. 3 and Fig. 4. In Fig. 5 we see that as the density decreases, the overall intensity of the scattered light increases. A similar behavior [57, 60] has been observed for measurements on the $F = 2 \rightarrow F' = 3$ hyperfine transition of ^{87}Rb . The effect is due to the collective nature of near resonance light scattering from a high density and cold atomic gas. Because the optical depth is so large for the highest density, light scattering occurs primarily from the outer surface of the sample. Relatively few atoms then contribute to the sample. For lower density the light can penetrate more deeply and a relatively larger number of atoms participate, leading to a larger signal.

B. Variations with spectral detuning from resonance

We now consider the variations of the scattered light signals as a function of detuning of the probe laser frequency from bare atomic resonance, where $\Delta = 0$. These data are recorded under conditions of a very weak probe laser, so that Zeeman optical pumping is negligible. For the steady state regime (as in the lowest probe intensity results of Fig. 3), this dependence is shown in Fig. 6. There we see that the spectral variations show a clear resonance behavior in a range of 3 to 4 γ about $\Delta = 0$, where γ is the $\sim 6 \text{ MHz}$ natural width of the atomic resonance. The solid line is a Lorentzian line profile, which well describes the resonance line shape, and yields a full width at half maximum of slightly larger than 10 MHz . A full-width greater than the natural width is expected, due to absorption broadening and due to the dipole-dipole interaction of the atoms under high density conditions. Selection of the Lorentzian line shape is arbitrary, but gives a decent fit to the data and a consistent way of estimating the full width under different experimental conditions. Within the spread of the data, a fit using a Gaussian line profile yields essentially the same full width at half maximum.

To further analyze the experimental data, we have extracted the full width at half maximum of the spectral profile as a function of time [57]. With reference to the lowest intensity results of Fig. 3, this is equivalent to making a slice on the time axis of 100 ns and recording the spectral profile as a function of detuning in this time window. Repeating this procedure for the full sequence of data over the $2.5 \mu\text{s}$ range of the probe excitation and

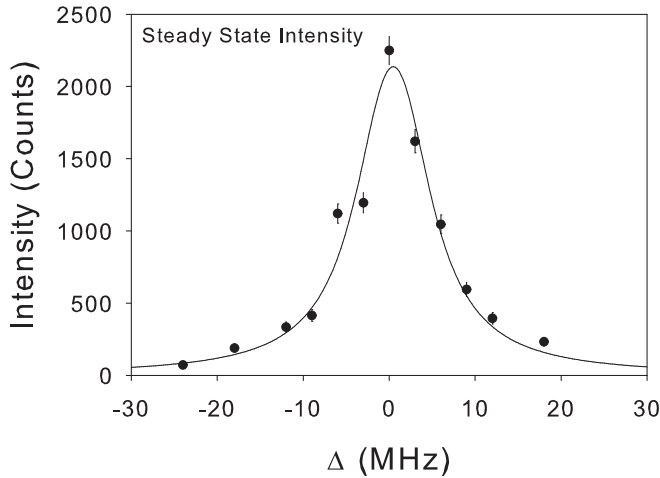


FIG. 6: Near-resonance spectral variation of the total scattered light intensity in the spectral vicinity of the $F = 1 \rightarrow F' = 0$ hyperfine transition.

decay signals yields the excitation spectrum shown in Fig. 7. There we see that the line width is very large for short times, rapidly decays to its steady state level (as in Fig. 6), and then sharply decreases again after the probe pulse is extinguished. For the short-time turn on of the excitation pulse single scattering dominates, and the line width can be estimated to be $\Delta_o = \gamma/2\sqrt{b_o - 1}$, where b_o is the on resonance transverse optical depth through the center of the cloud. For the experiments reported here $b_o = 40$, giving a full width of $\Delta_o = \gamma\sqrt{b_o - 1} \sim 37$ MHz, in very good agreement with the short time value of Fig. 6.

Upon turn off of the probe pulse the spectral width of the excitation spectrum decreases from its steady state value of about 10 MHz to a value on the order of the natural width. As in the spectral response upon turn-on of the probe pulse, the line shape here is also well fit by a Lorentzian form. However, we point out that the spectral width of the probe laser itself is about 1 MHz, and has a measured Gaussian power spectrum. This means that the widths determined by these measurements are slightly larger than that determined by the physical processes involved. In fact, the longest lived mode [57] for these samples corresponds to the so called Holstein mode, or the longest lived diffusive mode for the sample under study; the lifetime of this mode can be significantly smaller than the natural width of the transition.

IV. THEORY

In this section we present theoretical calculations for comparison with the steady state line shape of the excitation spectrum. In general, microscopic calculations for the cooperative scattering process for a macroscopic collection of atoms with a degenerate ground state is rather

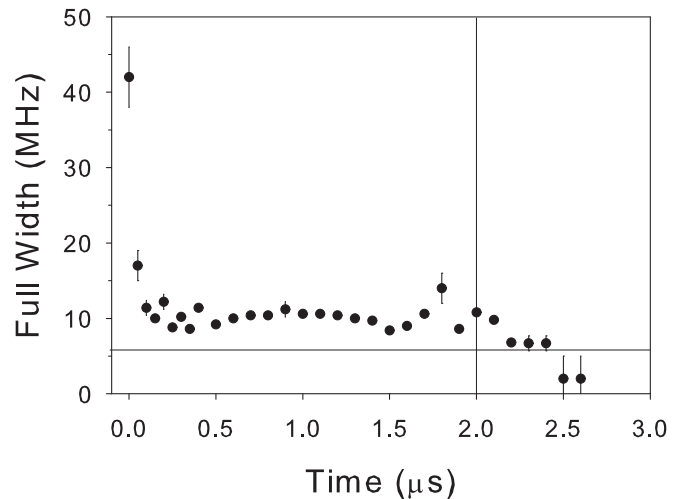


FIG. 7: Time evolution of the probe scattered light intensity on the $F = 1 \rightarrow F' = 0$ hyperfine transition. The atomic density is at its peak level for these measurements.

difficult because of the rapidly rising number of equations to be solved $d_e N d_g^{N-1}$, where d_e is the degeneracy of the atomic excited state and d_g is the degeneracy of the ground state. Here N is the number of atoms considered in the calculations. This makes practically impossible exact microscopic calculations for the scattering process and for its time-dependent fluorescence dynamics. In this section we present the results of our calculations of the scattering spectrum in the steady state regime, which are based on two complementary models of the self-consistent and approximate microscopic approaches, see Ref. [27], and discuss the results of our numerical simulations in the context of the data presented in the experimental part of the paper.

The self-consistent approach accepts the description of the scattering problem on the level of the macroscopic (i.e. mesoscopically averaged) Maxwell theory, where the dielectric susceptibility obeys an equation resulting from the self-consistent dynamics of the driving (probe) field and of the atomic dipoles. The crucial assumption is that groups of closely located atomic dipoles respond to the field cooperatively such that the longitudinal dipole-dipole interaction can be incorporated into the Lorentz-Lorenz local-field correction. For a low intensity of the driving field (where optical pumping can be neglected) the atoms equally populate the Zeeman sublevels and the medium is isotropic and can be parameterized by a single dielectric constant. If the atoms are homogeneously distributed in a spherical volume, then it is possible to express the scattering cross section by the standard solution of the Debye-Mie problem. In Fig. 8 we reproduce the spectral dependencies of the total cross section calculated for such a spherically symmetrical atomic system. The chosen radius of the sphere $30 \mu\text{m}$ is roughly scaled by the spot size where the probe beam crosses the atomic sample. We use the densities essentially less than in the

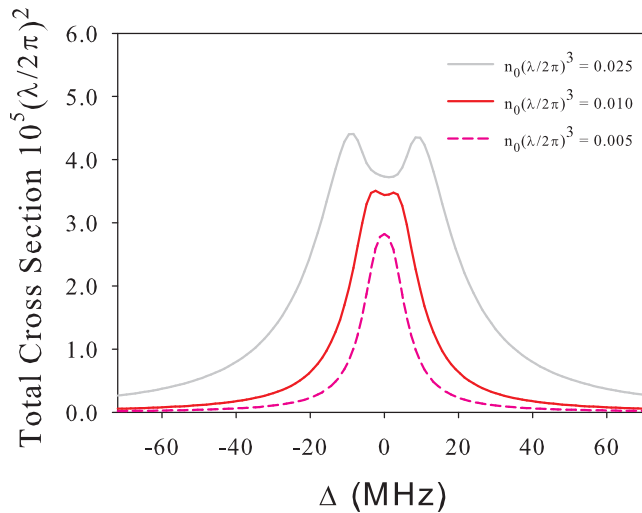


FIG. 8: The scattering cross section calculated in the Debye-Mie model for an atomic sample with radius $30 \mu\text{m}$. Atoms fill a sphere homogeneously with the density varying from 0.005 to 0.025.

peak point of the cloud to emphasize the importance of the contribution from the tail area of the Gaussian distribution in the experimental observation of the scattering process. The plotted dependencies demonstrate the smoothed spectral profile with a bandwidth qualitatively in agreement with the experimental data of Fig. 6. Note that there is a slight asymmetry in the spectral behavior related with the density effects which is a consequence of the spectral asymmetry of the dielectric permittivity. Because of the essential differences in geometries of this model and the experiment, which is a prolate double Gaussian distribution in experiment and spherically homogeneous in theory, we cannot make direct quantitative comparison of experimental and theoretical results but we can point out at least the qualitative agreement between both the data sets. We finally point out that the near resonance theoretical behavior is structured as a competition of longitudinal red shift and cooperative radiation blue shift but this effect is very likely masked by the uncertainty in experimental data.

We note that the time dynamics associated with the fluorescence decay can be also modeled in the framework of the self-consistent calculation scheme. However, this would require the complete Monte-Carlo simulations of the process with the Green's function formalism, see Ref. [22]. The scattered energy of the light scattered from a dense atomic cloud in the steady state regime emerges mainly from its surface area and the transient deviations for the widths of the fluorescence spectra reproduced in Fig. 7 could be verified by such a Monte-Carlo simulated and spectrally sensitive self-consistent calculations.

As we commented above, the microscopic calculations can be only approximately done for the considered transition. Here we reproduce the results of our calculations

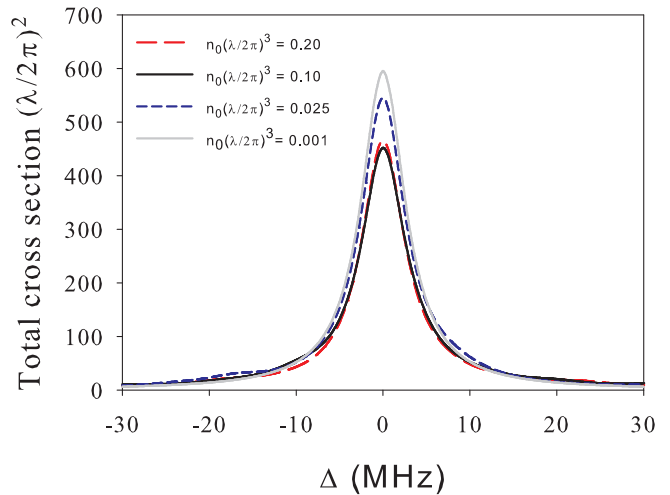


FIG. 9: The scattering cross section calculated microscopically for an ensemble consisting of one hundred atoms. Atoms have a spherically symmetrical Gaussian distribution with the peak density varying from $n_0\lambda^3 = 0.001$ to 0.2 and populating only one Zeeman sublevel.

based on the general formalism of the quantum scattering theory previously developed in Ref. [27] and present the data for the case of a sample consisting of one hundred atoms. For the typical experimentally attained atomic densities, which are less than $n_0\lambda^3 \lesssim 0.1$ in its peak value, in order to resolve the quasi-energy structure, associated with the longitudinal dipole-dipole interaction, it would be enough to take into consideration only a few nearest neighbors in the vicinity of each selected scatterer. This scheme were tested by us on a small number of atoms and it demonstrated reliable convergence, which reduces the number of equations to be solved to $d_e N d_g^{n-1}$, where n is the number of the neighboring atoms retained in the calculation.

In Fig. 9 we show the results of our calculations, which were done for $n = 4$ and for all the atoms populating one Zeeman sublevel. Let us point out here again that because of high degeneracy of the ground state our results cannot be statistically averaged over all the populated initial states. That means we cannot directly compare them on a one-to-one basis either with experiment or with the self-consistently calculated data. Instead, we rely on qualitative comparison among the results.

First, as was explained in Ref. [27], because of the presence of elastic Raman scattering channels there is no visible signature of either super- or sub-radiant Dicke-type exciton modes for the $F = 1 \rightarrow F' = 0$ transition. In contrast with $F = 0 \rightarrow F' = 1$ transition (where such states are normally predicted and discussed) in the $F = 1 \rightarrow F' = 0$ case all the resolvent poles are described as the resonances with a typical line width of about γ . Thus the presence of the cooperative longitudinal and radiative interactions manifest themselves in the smoothed

variation of the scattering spectrum associated with disorder and with the configuration dependence. The slight modulation of the experimental spectrum, which is suggested in the experimental data shown in Fig. 6 can be not only experimental uncertainty but can be also manifestation of the cooperativity and disorder effects. Second, we can point out that because of competition between near and far field interactions the microscopically calculated spectra have an asymmetry in respect to the atomic resonance line. The latter observation is in qualitative agreement with the predictions of the self-consistent model, which were pointed out above.

V. CONCLUSIONS

We have presented detailed experimental and theoretical results associated with scattering of light from an ultracold and highly dense gas of ^{87}Rb atoms. For radiation tuned in the spectral vicinity of the $F = 1 \rightarrow F' = 0$ hyperfine component of the D_2 line, we have studied the atomic density, probe laser detuning and probe laser intensity dependence of the scattered light intensity. The measured time dependence and steady state responses indicate that the light dynamics is strongly effected by Zeeman optical pumping in the lower energy $F = 1$ hyperfine component. However, for very low probe laser intensities,

Zeeman optical pumping can be made negligible; this has allowed for study of the steady state regime in the absence of optical pumping. Good results are obtained in comparison between the experimental results and theoretical calculations. The strong role of elastic Raman transitions also strongly suggests that this transition is not particularly suitable for searches for Anderson light localization in three dimensions.

VI. ACKNOWLEDGMENTS

We acknowledge Daniel Havey for informative discussions and contributions to the experimental line shape fitting. We appreciate financial support by the National Science Foundation (Grant Nos. NSF-PHY-0654226 and NSF-PHY-1068159), the Russian Foundation for Basic Research (Grant No. RFBR-CNRS 12-02-91056). D.V.K. would like to acknowledge support from the External Fellowship Program of the Russian Quantum Center (Ref. Number 86). We also acknowledge the generous support of the Federal Program for Scientific and Scientific-Pedagogical Personnel of Innovative Russia for 2009-2013 (Contract No. 14.B37.21.1938). A.S.S. would like to acknowledge support from the charitable foundation "Dynasty".

-
- [1] M.D. Havey, *Contemp. Phys.* 50, 587 (2009).
 - [2] H.J. Metcalf and P. van der Straten, *Laser Cooling and Trapping*, Springer, New York, 1999.
 - [3] R. Grimm, M. Weidemüller, and Y. Ovchinnikov, *Adv. Atom., Mol., and Opt. Phys.* 42, 95 (2000).
 - [4] C.J. Pethick and H. Smith, *Bose-Einstein Condensation in Dilute Gases*, Cambridge University Press, Cambridge, UK, 2002.
 - [5] S. Giorgini, L.P. Pitaevskii, and S. Stringari, *Rev. Mod. Phys.* 80, 1215 (2008).
 - [6] Dirk Bouwmeester, Artur Ekert, and Anton Zeilinger, *The Physics of Quantum Information*, Springer-Verlag, Berlin, Germany, 2001.
 - [7] M.D. Lukin, *Rev. Mod. Phys.* 75, 457 (2003).
 - [8] P.W. Milonni, *Fast Light, Slow Light, and Left-handed Light*, Taylor and Francis, New York, 2005.
 - [9] M. Fleischhauer, A. Imamoglu, and J.P. Marangos, *Rev. Mod. Phys.* 77, 633 (2005).
 - [10] Lene Vestergaard Hau, *Nature Photonics* 2, 451 (2008).
 - [11] D.A. Braje, V. Balic, G.Y. Yin, and S.E. Harris, *Phys. Rev. A* 68, 041801 (2003).
 - [12] S. Ospelkaus, A. Peer, K.-K. Ni, J. J. Zirbel, B. Neyenhuis, S. Kotochigova, P. S. Julienne, J. Ye, and D. S. Jin, *Nature Phys.* 4, 622 (2008).
 - [13] G. K. Campbell, A. D. Ludlow, S. Blatt, J. W. Thomsen, M. J. Martin, M. H. de Miranda, T. Zelevinsky, M. M. Boyd, J. Ye, S. A. Diddams, T. P. Heavner, T. E. Parker, and S. R. Jefferts, *Metrologia* 45, 539 (2008).
 - [14] Jun Ye, S. Blatt, M. M. Boyd, S. M. Foreman, E. R. Hudson, Tetsuya Ido, B. Lev, A. D. Ludlow, B. C. Sawyer, B. Stuhl, T. Zelinsky, *Int. J. Modern Phys. D* 16, 2481 (2007).
 - [15] Steven Rolston, *Physics* 1, 2 (2008).
 - [16] Thomas C. Killian, *Science* 316, 705 (2007).
 - [17] The entire issue, *New J. Phys.* 11 (2009), focuses on recent advances and opportunities in ultracold molecular physics. See particularly, Lincoln D. Carr and Jun Ye, *New J. Phys.* 11, 055009 (2009).
 - [18] Matthias Weidemüller and Claus Zimmermann, *Interactions in Ultracold Gases*, Wiley-VCH, Germany, 2003.
 - [19] M. Fleischhauer and M. D. Lukin, *Phys. Rev. A* 65, 022314 (2002).
 - [20] Y. O. Dudin, S. D. Jenkins, R. Zhao, D. N. Matsukevich, A. Kuzmich, and T. A. B. Kennedy, *Phys. Rev. Lett.* 103, 020505 (2009).
 - [21] G. Labeyrie, *Mod. Phys. Lett. B* 22, 73 (2008).
 - [22] D.V. Kupriyanov, I.M. Sokolov, C.I. Sukenik, and M.D. Havey, *Laser Phys. Lett.* 3, 223 (2006).
 - [23] Mark D. Havey and Dmitriy V. Kupriyanov, *Phys. Scr.* 72, C30 (2005).
 - [24] R. Kaiser and M.D. Havey, *Optics and Photonics News* 16, 38 (2005).
 - [25] P. W. Anderson, *Phys. Rev.* 109, 1492 (1958).
 - [26] E. Akkermans, A. Gero, and R. Kaiser, *Phys. Rev. Lett.* 101, 103602 (2008).
 - [27] I.M. Sokolov, M.D. Kupriyanova, D.V. Kupriyanov, and M.D. Havey, *Phys. Rev. A* 79, 053405 (2009); A. S. Sheremet, A. D. Manukhova, N. V. Larionov, and D. V. Kupriyanov *Phys Rev A* 86, 043414 (2012).
 - [28] Ya. A. Fofanov, A.S. Kuraptsev, I.M. Sokolov, and M.D.

- Havey, Phys. Rev. A 84, 53811 (2011).
- [29] I.M. Sokolov, D.V. Kupriyanov, and M.D. Havey, JETP 112, 246 (2011).
 - [30] D.S. Wiersma, P. Bartolini, Ad Lagendijk, and R. Righini, Nature 390, 671 (1997).
 - [31] A.A. Chabanov, M. Stoytchev, and A.Z. Genack, Nature 404, 850 (2000).
 - [32] M. Storzer, P. Gross, C.M. Aegerter, and G. Maret, Phys. Rev. Lett. 96, 063904 (2006).
 - [33] C.M. Aegerter and G. Maret, *Coherent backscattering and Anderson localization of light*, in Progress in Optics 52, 1 (2009).
 - [34] Marlin O. Scully, Phys. Rev. Lett. 102, 143601 (2009).
 - [35] A.A. Svidzinsky, J. Chang, and M.O. Scully, Phys. rev. Lett. 100, 160504 (2008).
 - [36] L. Froufe-Prez, W. Guerin, R. Carminati, and R. Kaiser Phys. Rev. Lett. 102, 173903 (2009).
 - [37] T. Bienaime, R. Bachelard, N. Piovella and R. Kaiser, Fortschr. Phys. doi: 10.1002/prop.201200089 (2012).
 - [38] T. Bienaime, M. Petruzzio, D. Bigerni, N. Piovella and R. Kaiser, J. Mod. Opt. 58, 1942 (2011).
 - [39] S. Bux, E. Lucioni, H. Bender, T. Bienaime, K. Lauber, C. Stehle, C. Zimmermann, S. Slama, Ph.W. Courteille, N. Piovella and R. Kaiser, J. Mod. Opt. 57, 1841 (2010).
 - [40] T. Bienaime, S. Bux, E. Lucioni, Ph.W. Courteille, N. Piovella, R. Kaiser Phys. Rev. Lett. 104, 183602 (2010).
 - [41] Ph.W. Courteille, S. Bux, E. Lucioni, K. Lauber, T. Bienaime, R. Kaiser, N. Piovella Eur. Phys. J. D 58, 69 (2010).
 - [42] Hui Cao, *Lasing in Disordered Media*, in Progress in Optics 45, (2003).
 - [43] D.S. Wiersma, Nature Phys. 4, 359 (2008).
 - [44] C. Conti and A. Fratalocchi, Nature Phys. 4, 794 (2008).
 - [45] L. Froufe-Perez, W. Guerin, R. Carminati and R. Kaiser Phys. Rev. Lett. 102, 173903 (2009).
 - [46] W. Guerin, N. Mercadier, D. Brivio and R. Kaiser, Optics Exp. 17, 14 (2009).
 - [47] W. Guerin, N. Mercadier, F. Michaud, D. Brivio, L. S. Froufe-Prez, R. Carminati, V. Ereemeev, A. Goetschy, S. E. Skipetrov, R. Kaiser, J. Opt. A 12, 024002 (2010).
 - [48] M.A. Nielsen and I.L. Chuang, *Quantum Computation and Quantum Information* (Cambridge University Press, 517, 2000).
 - [49] H.-J. Briegel, W. Dur, J.I. Cirac and P. Zoller, Phys. Rev. Lett. 81, 5932 (1998).
 - [50] L.-M. Duan, M.D. Lukin, J.I. Cirac and P. Zoller, Nature 414, 413 (2001).
 - [51] T. Bienaime, N. Piovella and R. Kaiser, Phys. Rev. Lett. 108, 123602 (2012).
 - [52] V.M. Datsyuk, I.M. Sokolov, D.V. Kupriyanov, and M.D. Havey, Phys. Rev. A 77, 033823 (2008).
 - [53] V.M. Datsyuk, I.M. Sokolov, D.V. Kupriyanov, and M.D. Havey, Phys. Rev. A 74, 043812 (2006).
 - [54] I.M. Sokolov, D.V. Kupriyanov, R.G. Olave, and M.D. Havey, J. Modern Optics 57, 1833 (2010).
 - [55] L.V. Gerasimov, I.M. Sokolov, D.V. Kupriyanov, R.G. Olave, and M.D. Havey, JOSA B 28, 1459 (2011).
 - [56] L.V. Gerasimov, I.M. Sokolov, D.V. Kupriyanov, and M.D. Havey, J. Phys. B: At. Mol. Opt. Phys. 45 124012 (2012).
 - [57] S. Balik, A.L. Win, M.D. Havey, I.M. Sokolov, and D.V. Kupriyanov, arXiv:0909.1133v3 [quant-ph].
 - [58] S. Balik, A.L. Win, and M.D. Havey, Phys. Rev. A 80, 023404 (2009).
 - [59] For an ellipsoidal Gaussian atom distribution of sizes r_o and z_o and peak density n_o , $n(r) = n_o e^{-r^2/2r_o^2 - z^2/2z_o^2}$. The total number of atoms is $N = (2\pi)^{3/2} n_o r_o^2 z_o$ and the peak transverse (longitudinal) optical depth is $b_t = \sqrt{2\pi} n_o \sigma_o r_o$ ($b_l = \sqrt{2\pi} n_o \sigma_o z_o$). σ_o is the weak field resonance light scattering cross section. The peak total cross-section is given by $\frac{2F'+1}{2F+1} \frac{\lambda^2}{2\pi}$.
 - [60] I.M. Sokolov, A.S. Kuraptsev, D.V. Kupriyanov, M.D. Havey and S. Balik J. Modern Optics, DOI:10.1080/09500340.2012.733431 (2012).